Progress in Natural Science: Materials International 29 (2019) 124–128

HOSTED BY

ELSEVIER

Contents lists available at ScienceDirect

Progress in Natural Science: Materials International

journal homepage: www.elsevier.com/locate/pnsmi

Boosting charge collection efficiency via large-area free-standing Ag/ZnO core-shell nanowire array electrodes

Yuyi Feng[a,b], Paul Kim[c], Clayton A. Nemitz[d], Kwang-Dae Kim[b], Yoonseok Park[e], Karl Leo[e], James Dorman[f], Jonas Weickert[b], Yongtian Wang[a,**], Lukas Schmidt-Mende[b,*]

[a] School of Optics and Photonics, Beijing Institute of Technology, 100081 Beijing, China
[b] Department of Physics, University of Konstanz, 78467 Konstanz, Germany
[c] Chemical and Biomolecular Engineering, University of California, 94720 Berkeley, USA
[d] Department of Physics and Astronomy, University of North Carolina, Chapel Hill, 27516 NC, USA
[e] Dresden Integrated Center for Applied Physics and Photonic Materials (IAPP), Dresden University of Technology, 01062 Dresden, Germany
[f] Chemical Engineering Department, Louisiana State University, Baton Rouge, 70803 LA, USA

ARTICLE INFO

Keywords:
Vertically aligned nanowires
Silver
Core-shell
Charge collection efficiency
Light harvesting
Semi-transparent organic solar cells

ABSTRACT

Hybrid nanostructures, comprising of a metal core and a semiconductor shell layer, show great potential for a new generation of low-cost solar cells due to their unique electronic and optical properties. However, experimental results have fallen far short of the ultra-high efficiency (i.e. beyond Shockley-Queisser limit) predicted by theoretical simulations. This limits the commercial application of these materials. Here, a non-transparent organic solar cell with an array of Ag/ZnO nanowires has been experimentally fabricated to increase the internal quantum efficiency (IQE) by a factor of 2.5 compared to a planar counterpart. This result indicates a significant enhancement of charge collection efficiency due to the ultrafast Ag nanowire channels. This hybrid nanostructure can also serve as a perfect back reflector for semi-transparent solar cells, which can result in enhanced light absorption by a factor of 1.8 compared to the reference samples. The enhanced charge collection and light absorption can make these Ag/ZnO nanostructures available for the application of modern optoelectronic devices.

1. Introduction

Nanostructures enable unprecedented control over the charge transport and light propagation [1–6], opening new avenues for applications in optoelectronic devices. One of the most intensively studied materials is the vertically-aligned nanowire array. These nanowire materials are of special interest to next-generation photovoltaic devices [5,7–9], due to their unusual charge collection channels and light management. Despite previous nanowire arrays being composed of a single semiconductor (e.g. TiO_2, ZnO), poor-performing solar cells were obtained due to severe surface charge recombination [10]. It was shown that the surface recombination could be greatly reduced by adopting core-shell nanostructures [11–13]. For example, a semiconductor core (e.g. ZnO) is coated with a semiconductor shell (e.g. TiO_2, Al_2O_3) in order to further increase distance between electron-hole pairs while simultaneously promoting charge extraction along the axis of the nanowire [14,15]. This phenomenon was further employed in the doped TiO_2 core-shell wires to amplify the electron mobility in the core of the wire, without forming a recombination center along the internal interface [15,16].

However, the metal-oxide semiconductors (e.g. TiO_2, ZnO) are not highly conductive. To improve the performance of solar cells, a hybrid core-shell nanostructure with enhanced charge mobility, one of which is a metal nanowire core (such as Ag) with a semiconductor shell layer, could provide an optimal electrode [15]. There have been many theoretical efforts towards analysis and simulation of incorporating metal nanowires or metal-nanowire/semiconductor core-shell arrays into solar cells [17–22], demonstrating the potential of outstanding performance in devices. Nevertheless, the experimental results fall far short of the corresponding predicted efficiencies, due to the complexity of chemical reactions, nano-engineering bottlenecks, and the inability of recent theoretical modeling to account for all of the optical, electrical and morphological contributions [23,24].

This paper reports on the successful fabrication of organic solar cells

* Corresponding author.
** Corresponding author.
E-mail addresses: wyt@bit.edu.cn (Y. Wang), lukas.schmidt-mende@uni-konstanz.de (L. Schmidt-Mende).

https://doi.org/10.1016/j.pnsc.2019.03.002
Received 20 December 2018; Received in revised form 28 February 2019; Accepted 5 March 2019
Available online 23 April 2019

based on metal/semiconductor nanowire arrays. The large-area free-standing silver nanowire arrays were fabricated by using a low-cost, bottom-up, template-assisted electrochemical approach. The ZnO shell layer was coated by a multi-cycle spin-coating method. Such electrodes were then incorporated into the typical bulk heterojunction P3HT:PCBM (poly(3-hexylthiophene): [6,6]-phenyl-C61-butyric acid methyl ester) organic solar cells. In non-transparent solar cells, the internal quantum efficiency (IQE) was significantly improved by a factor of 2.5 compared to the planar counterparts, indicating a significant enhancement of charge collection efficiency. Furthermore, in order to make full use of the light harvesting properties of the nanostructures, while eliminating the front-reflection by the Ag nanowire arrays, a semi-transparent architecture was prepared. The semi-transparent nanostructured architecture showed promising absorption enhancement over the entire related spectral range, with a maximum enhancement factor of 1.8 at 627 nm. The probability analysis of the charge collection confirmed that the nanostructures improve the efficiency of the charge collection, even though the device structures are not yet fully optimized.

2. Experimental

2.1. Materials and device fabrication

The schematics of the planar and nanowire solar cells are shown in Fig. 1a and b, respectively. To fabricate nanowire solar cells, an anodic aluminum oxide (AAO) template-assisted electrochemical deposition method was used to obtain the silver nanowire arrays over large commercial indium-tin-oxide (ITO) coated (180 nm with 10 Ω/sq) glass substrates (14 × 14 × 1.1 mm, Praezisions Glas & Optik, Germany), as shown in Fig. 1c. The AAO was prepared on an ITO substrate, where a 5 nm Ti adhesion layer and a 2 nm Au layer were used to improve the nucleation for the following deposition of Ag nanowires. The typical dimensions of the silver nanowires used in this work are: ~80 nm in diameter, ~133 nm in period, and 100–250 nm long. The detailed nanowire fabrication process has been described in our previous work [15]. To remove some overgrown silver structures and contamination (e.g. residual K^+, etc. left over from the chemical synthesis) on the nanowire samples, tip sonication (Ultraschall-Homogenisator mit HF-Generator GM3200) was used on the AAO-embedded nanowires in isopropanol (pulse on = 5 s with an amplitude of 45%; pulse off = 15 s; duration = 5 min; a distance of around 2 mm between the tip and sample surface). This procedure was followed by immersion in 0.1 M NaOH aqueous solution for 50 min to remove the AAO templates, cleaning with deionized water, ethanol (purity 99.8%), and isopropanol (purity 99.9%), and carefully drying with a weak stream of dry N_2. Next, the electron selective layer, ZnO (ca. 30 nm), was spin-coated. In order to quasi-conformally cover the silver nanowire arrays, as depicted in Fig. 1d, we have developed a four-cycle spin-coating procedure. Specifically, the prepared precursor solution (40 µl; 0.5 M [Zn $(CH_3COO)_2{\cdot}2H_2O$ in 2-methoxyethanol solvent with 3 vol% of ethanolamine as a stabilizer; Sigma-Aldrich]) was dropped onto the nanowire samples, and remained there for 1 min to ensure that the precursor filled the voids between nanowires. Afterwards, the samples were spin-coated at 5000 rpm for 40 s (acceleration 1000 rpm/s). The samples with the ZnO shell were then annealed at 250 °C for 10 min in air. This procedure was repeated for four cycles to achieve a nearly conformal, pin-hole free coating of the ZnO layer. Next, the active layer, P3HT:PCBM (ca. 400 nm) was spin-coated. To ensure the best infiltration of the polymer into the nanowire arrays, the samples were pre-treated in chlorobenzene for 4 min before spin-coating P3HT:PCBM (80 µl; 30 mg P3HT (Rieke, MW = 69 kDa) and 24 mg PCBM (Nano-C) in 1 ml chlorobenzene) on top in a first step at 50 rpm for 2 min. After that, the spin speed was increased to 1500 rpm (acceleration 500 rpm/s) for 1 min to form a homogeneous layer (Fig. S1 in the Supporting Information). The successful infiltration of P3HT:PCBM can be seen in Fig. 1d. Finally, a hole-selective WO_3 layer (5 nm) and then an Ag back contact (120 nm) were thermally evaporated on top of the polymer film. The overlap between the ITO and the evaporated Ag electrode forms an active area of 18 mm^2. For the reference planar solar cells (Fig. 1a), all fabrication procedures were kept identical starting with the spin-coating of the ZnO layer on a planar substrate.

2.2. Device characterization

In solar cell characterization, a shadow mask was used, which had a slightly smaller area (12.5 mm^2) than the solar cell pixel (18 mm^2), to minimize edge effects and to precisely define the photoactive area during the measurement [25]. For the non-transparent solar cells, 9 independent batches of samples were made, with 68 working nanostructured pixels overall. Only ~20% of the nanostructured devices worked in solar cells due to shorting issues caused by overgrown Ag clusters from the electrodeposition of the Ag nanowires [15], where the removal of this overgrown Ag was not successful. Internal quantum

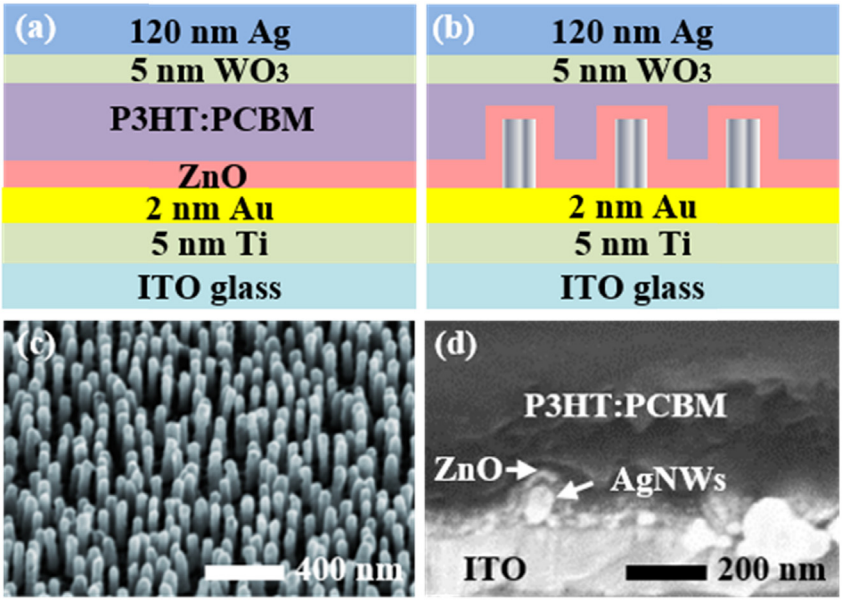

Fig. 1. (a–b) Schematic illustrations of the non-transparent planar and Ag/ZnO core-shell nanowire organic solar cells, respectively. (c) Typical scanning electron spectroscopy (SEM) side view of the free-standing silver nanowire arrays at a stage degree of 54°. (d) A cross-sectional SEM image of the Ag/ZnO core-shell nanowire organic solar cells without the top electrodes at a stage degree of 54°.

efficiency (IQE) was indirectly obtained from the ratio between the external quantum efficiency (EQE) and the total absorption (Abs) as IQE (λ) = EQE (λ)/Abs (λ). EQE measurements were performed under monochromatic illumination (LOT Oriel LS0106 150 W Xe-lamp combined with an OMNI Lambda 300 monochromator) using a Fraunhofer ISE certified Si reference solar cell. Total absorption (Abs) measurements were conducted using a commercial UV–vis–NIR spectrometer (Cary 5000 series, Agilent Technologies) in a double beam mode. In this case, in order to ensure the measurement accuracy, the overlap between the ITO and evaporated metal electrode was made almost as large as the whole substrate, such that the projected beam spot (ca. 4 mm × 3 mm) was inside of the active area. The samples were placed in the middle of an integrating sphere with an angle of incidence (AOI) of 10°, in such a way that the direct reflected light on the sample surface could not escape from the integrating sphere. The charge collection probability (P_{CC}) was extracted from the current density-voltage (J–V) measurements via $P_{CC} = J(V)/J_{sat}$, where J_{sat} is the reverse saturation current density, where almost all charge carriers are swept out and collected by the electrodes [26,27]. In our case, the P_{CC} was normalized at the saturated reverse voltage of −0.6 V. Current density-voltage (J-V) measurements were carried out using a Keithley 2400 SourceMeter controlled by a Matlab program. The solar cells were illuminated by a LOT Oriel LS0106 solar simulator (a 1000 W Xe-Lamp combined with an AM1.5G filter). The light intensity was calibrated with a Fraunhofer ISE certified Si reference solar cell and adjusted to around 1 sun.

3. Results and discussion

The external quantum efficiency (EQE), i.e. photon-to-electron conversion efficiency, of an organic solar cell can be described by the product of the efficiency (η) of each single process (depicted in Fig. 2a) involved from light absorption to charge collection as below:

$$EQE(\lambda) = \eta_A(\lambda)\bullet\eta_{ED}(\lambda)\bullet\eta_{EDis}(\lambda)\bullet\eta_{CC}(\lambda). \quad (1)$$

where η_A represents the absorption efficiency, in which the organic materials absorb light, and the electrons are excited from HOMO levels (highest occupied molecular orbitals) to LUMO levels (lowest unoccupied molecular orbitals), resulting in the generation of strongly bounded electron-hole pairs, namely excitons; η_{ED} represents the exciton diffusion efficiency, i.e. the fraction of the excitons diffusing to the donor/acceptor interface; η_{EDis} represents the exciton dissociation efficiency, i.e. the fraction of the diffused excitons being dissociated into free charge carriers by the built-in energy offset at the donor/acceptor interface [28]; η_{CC} represents the charge collection efficiency, i.e., the fraction of the free charge carriers being collected by the respective electrodes.

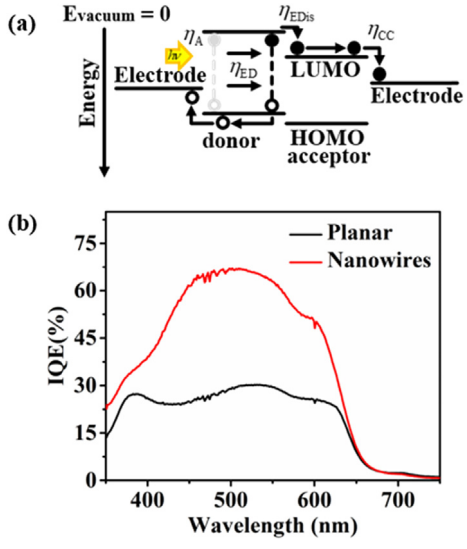

Fig. 2. (a) Schematic diagram of the working principles of typical organic solar cells, where η_A is the absorption efficiency, η_{ED} is the exciton diffusion efficiency, η_{EDis} is the exciton dissociation efficiency, and η_{CC} is the charge collection efficiency. (b) Internal quantum efficiency (IQE) for the non-transparent planar (black) and Ag/ZnO core-shell nanowire (red) solar cells, under short circuit condition without background illumination.

Moreover, the internal quantum efficiency, i.e. absorbed photon-to-electron, can be written as below:

$$IQE(\lambda) = \eta_{ED}(\lambda)\bullet\eta_{EDis}(\lambda)\bullet\eta_{CC}(\lambda). \quad (2)$$

Fig. 2b shows the IQE spectra of both planar and nanostructured non-transparent organic solar cells (with the best of the nanostructured pixels selected). It can be observed that the nanostructured solar cells show impressive enhanced IQE compared to the planar counterparts over the whole wavelength range (350–650 nm), with a maximum enhancement by a factor of 2.5 at 455 nm. From Equation (2), the enhanced IQE could be explained either by enhanced charge collection efficiency (η_{CC}) through the direct Ag/ZnO nanowire channels, or by changed morphology of polymers on the nanostructured electrode, which is assumed to be a minor effect. The reason is that there is no notable difference in morphology observed from SEM analysis, together with good exciton diffusion and exciton dissociation efficiencies η_{ED} • η_{EDis}.

However, the power conversion efficiency of nanostructured solar cells is 31% lower than that of the planar counterparts. One example of the J-V curves and the analysis of V_{OC} and FF is demonstrated in the Supporting Information (Fig. S2 and Table S1). To understand the reason for one of the major limiting factors, the current density of short circuit J_{SC}, the EQE and total absorption of the devices were compared, as shown in Fig. 3. It can be seen that in the spectral region below 400 nm, there is stronger absorption in the nanostructured devices than the planar devices (Fig. 3b), which might be due to the plasmonic

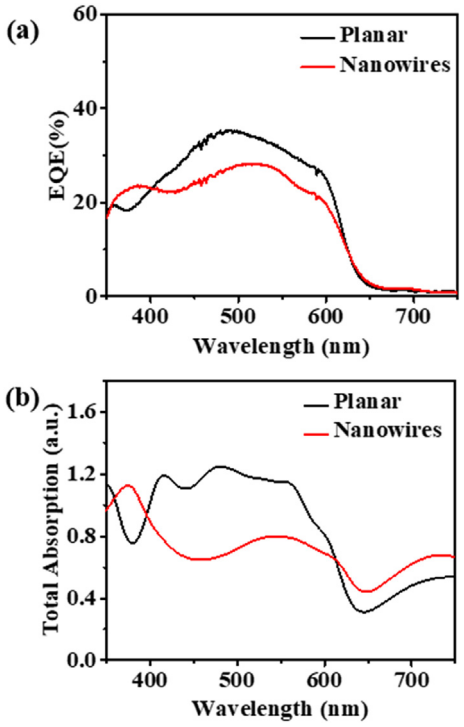

Fig. 3. (a) External quantum efficiency (EQE) for the non-transparent planar (black) and Ag/ZnO core-shell nanowire (red) organic solar cells, under short circuit condition without background illumination. (b) Total absorption spectra for the non-transparent planar (black) and Ag/ZnO core-shell nanowire (red) organic solar cells.

enhancement of the Ag nanowire arrays [15,29], leading to higher EQE (Fig. 3a). However, in the broader spectral region from 400 nm to 650 nm, both EQE and absorption of nanostructured devices are considerably lower than the planar counterparts, with a maximum decrease of 26% at 467 nm for EQE and a maximum decrease of 47% at 475 nm for absorption. It can be found that the dominating reason for this lower current are optical losses due to strong front-reflection by the dense Ag nanowire arrays, as Ag has the highest reflectivity among all metals [30–32]. Considerably lower light intensity is coupled into the nanostructured devices. We further noticed that four distinguished peaks in planar devices reduce to two in nanostructured devices (Fig. 3b, 350–650 nm), indicating that the nanostructures suppress the resonant Fabry-Perot cavity modes [33,34].

Although the nanostructured non-transparent solar cells present high IQE, the absorption measurement (Fig. 3b) demonstrates that the front positioned Ag nanostructured electrodes reflect a considerable amount of light, with an overall decrease of 23% (the integral in 350–650 nm) compared to the planar counterparts, which is consequently not contributing to the current generation. Although the absorbed photon-to-electron conversion is very efficient, the optical loss from the nanostructures' front reflection needs to be addressed to achieve clear benefits from such nanostructured devices.

One initial attempt to address the optical loss problem was to change the architecture from the conventional non-transparent structure to a semi-transparent structure by replacing the planar Ag electrode (120 nm) with a thin transparent top electrode of 10 nm multilayers (Al/Ca:Ag blend), with a 60 nm wide-band-gap Alq_3 organic capping layer, as depicted in Fig. 4a. The fabrication process and properties of this transparent electrode have been described previously [35]. The semi-transparent architecture with a nanostructured Ag bottom electrode serves as an excellent back reflector, and increases the optical path of light inside the device due to its nanostructure. Fig. 4b shows the comparison of planar and nanostructured solar cells (~250 nm long of AgNWs) under bottom illumination through ITO and top illumination through Ca:Ag blend, respectively. As expected, in the case of bottom illumination, the light absorption of the nanostructured device was lower than the planar counterparts due to the front-reflection effect of the nanostructured Ag electrode (Fig. 4b – upper graph). However, in the case of top illumination, the light absorption in the device with nanostructured electrode was significantly higher than that without nanostructuring in the main spectral range from 350 to 650 nm, with a maximum enhancement by a factor of 1.8 at 627 nm (Fig. 4b - lower graph). Furthermore, the comparison between the bottom- and top-illuminated nanostructured samples (Fig. 4b - two red curves) reveals that the light absorption was dramatically improved, with a maximum increase by a factor of 2.8 at 601 nm. This result indicates that the semi-transparent architecture is a promising approach with two main advantages: i) excellent charge collection, and ii) light scattering increasing the optical path-length in the device.

Fig. 4c shows the extracted charge collection probability calculated from the J-V curves of the best pixel in another independent batch of semi-transparent solar cells (~130 nm long AgNWs, shown in the Supporting Information Fig. S3 and Table S2) under both top and bottom illumination. In both cases, the charge collection probability of nanostructured devices outperformed the planar counterparts in a large range of biased voltages, including the voltage at maximum power point. Near V_{OC} (~0.4 V), the charge collection probability was lower than the planar devices, which is due to the low V_{OC} of the nanostructured solar cells. The reason for this lower V_{OC} is assumed to be due to the insertion of silver, changing the energy-level alignment in the device [36,37], despite the improved charge collection efficiency. If the V_{OC} can be further improved (e.g. by additional interface modifications), the charge collection probability in devices with nanostructured electrodes would outperform the planar devices over the complete voltage range.

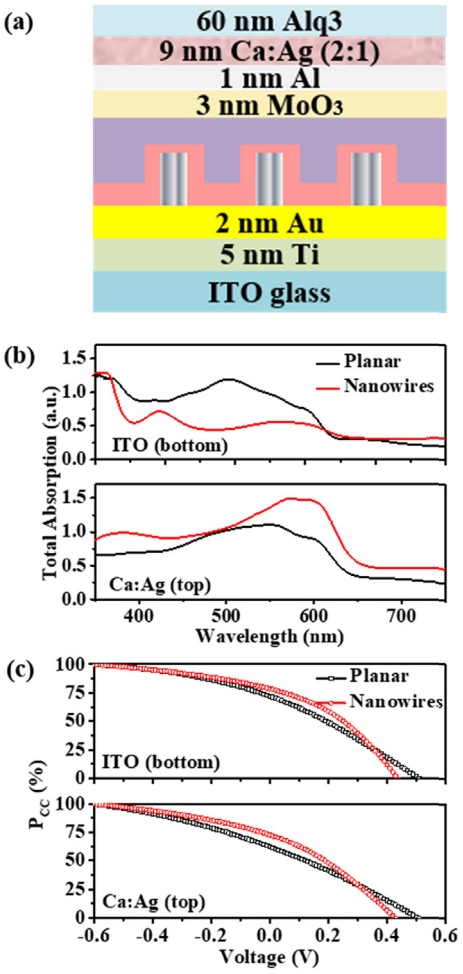

Fig. 4. (a) Schematic illustration of the semi-transparent Ag/ZnO core-shell nanowire organic solar cells. (b) Total absorption spectra for the semi-transparent planar (black) and Ag/ZnO core-shell nanowire (red) organic solar cells under bottom illumination through ITO glass and top illumination through Ca:Ag electrode, respectively. (c) Charge collection probability for the semi-transparent planar (black) and Ag/ZnO core-shell nanowire (red) organic solar cells under bottom illumination through ITO glass and top illumination through Ca:Ag electrode, respectively. The P_{CC} was normalized at the saturated reverse voltage of −0.6 V.

4. Conclusion

An extensible electrochemical fabrication method for large-area Ag nanowire arrays has been successfully applied to electrode materials for organic solar cells. Using a multi-cycle spin-coating, Ag/ZnO core-shell nanowire arrays have been formed. These nanowire arrays have been successfully infiltrated by a donor-acceptor blend. The analysis results of the non-transparent solar cells show that the nanostructured electrodes can significantly enhance the charge collection efficiency. Furthermore, the results also demonstrate the implementation of the nanostructured electrodes into the semi-transparent solar cells. This could be appealing for colorful solar windows integrated into buildings and vehicles [38–40]. The improved light harvesting ability of nanostructures indicates that an excellent back reflector formed can enhance the internal light path when illuminated from the semi-transparent top electrode. Although further optimization regarding the thickness of the transparent top electrode, the organic semi-conductor layer, and passivation of the nanowires still need to be done, the observed charge collection and light harvesting properties indicate that the Ag/ZnO nanostructured electrodes have great potential in optoelectronic devices.

Acknowledgements

Y. F. acknowledges the support of the China Scholarship Council, the bridge scholarship by the Equal Opportunity Council of the University of Konstanz, and the China Postdoctoral Science Foundation. P. K. acknowledges the DAAD RISE Foundation, Alan S. Tetelman 1958 Fellowships for International Research in the Sciences and Saybrook College Richter Summer Fellowship. C. A. N acknowledges the Brown Family Internship Grant. K. D. K. acknowledges the Basic Science Research Program through the National Research Foundation of Korea funded by the Ministry of Education, Science and Technology (No. NRF-2013R1A6A3A03057669), and the REFINE research consortium of the Carl Zeiss Foundation. Y. P. acknowledges the Deutsche Forschungsgemeinschaft, PA 3154/1-1. K. L. acknowledges Canadian Institute for Advanced Research. J. A. D. acknowledges the Alexander von Humboldt Foundation for support through a postdoc fellowship. J. W. acknowledges funding by the Carl Zeiss Foundation through a postdoc fellowship. Y. W. acknowledges the support of the NSFC Project of International Cooperation and Exchanges (No. 61420106014).

Appendix A. Supplementary data

Supplementary data to this article can be found online at https://doi.org/10.1016/j.pnsc.2019.03.002.

References

[1] J. Weickert, R.B. Dunbar, H.C. Hesse, W. Wiedemann, L. Schmidt-Mende, Adv. Mater. 23 (2011) 1810–1828.
[2] N. Ali, A. Hussain, R. Ahmed, M.K. Wang, C. Zhao, B.U. Haq, Y.Q. Fu, Renew. Sustain. Energy Rev. 59 (2016) 726–737.
[3] Z. Wang, D. Cao, R. Xu, S. Qu, Z. Wang, Y. Lei, Nano Energy 19 (2016) 328–362.
[4] H.P. Wang, H. He Jr., Adv. Energy Mater. 7 (2017) 1602385.
[5] A. Polman, M. Knight, E.C. Garnett, B. Ehrler, W.C. Sinke, Science 352 (2016) aad4424.
[6] J. Wang, S. Liu, X. Meng, G. Zhu, M. Shi, L. Liu, J. Zhang, W. Yang, W. Fu, H. Yang, Electrochim. Acta 258 (2017) 858–865.
[7] Z. Fan, H. Razavi, J.-w. Do, A. Moriwaki, O. Ergen, Y.-L. Chueh, P.W. Leu, J.C. Ho, T. Takahashi, L.A. Reichertz, S. Neale, K. Yu, M. Wu, J.W. Ager, A. Javey, Nat. Mater. 8 (2009) 648.
[8] Y. Cui, D. van Dam, S.A. Mann, N.J.J. van Hoof, P.J. van Veldhoven, E.C. Garnett, E.P.A.M. Bakkers, J.E.M. Haverkort, Nano Lett. 16 (2016) 6467–6471.
[9] J. Zhu, Z. Yu, G.F. Burkhard, C.-M. Hsu, S.T. Connor, Y. Xu, Q. Wang, M. McGehee, S. Fan, Y. Cui, Nano Lett. 9 (2008) 279–282.
[10] P. Docampo, A. Ivaturi, R. Gunning, S. Diefenbach, J. Kirkpatrick, C.M. Palumbiny, V. Sivaram, H. Geaney, L. Schmidt-Mende, M.E. Welland, J. Mater. Chem. A 1 (2013) 12088–12095.
[11] Y. Sun, X. Yang, H. Zhao, R. Wang, Prog. Nat. Sci-Mater. 27 (2017) 157–168.
[12] Q. Zhao, M. Ji, H. Qian, B. Dai, L. Weng, J. Gui, J. Zhang, M. Ouyang, H. Zhu, Adv. Mater. 26 (2014) 1387–1392.
[13] J. Liu, J. Feng, J. Gui, T. Chen, M. Xu, H. Wang, H. Dong, H. Chen, X. Li, L. Wang, Z. Chen, Z. Yang, J. Liu, W. Hao, Y. Yao, L. Gu, Y. Weng, Y. Huang, X. Duan, J. Zhang, Y. Li, Nano Energy 48 (2018) 44–52.
[14] M. Law, L.E. Greene, A. Radenovic, T. Kuykendall, J. Liphardt, P. Yang, J. Phys. Chem. B 110 (2006) 22652–22663.
[15] Y. Feng, K.-D. Kim, C.A. Nemitz, P. Kim, T. Pfadler, M. Gerigk, S. Polarz, J.A. Dorman, J. Weickert, L. Schmidt-Mende, J. Electrochem. Soc. 163 (2016) D447–D452.
[16] J.A. Dorman, J. Weickert, J.B. Reindl, M. Putnik, A. Wisnet, M. Noebels, C. Scheu, L. Schmidt-Mende, J. Phys. Chem. C 118 (2014) 16672–16679.
[17] R.B. Dunbar, T. Pfadler, L. Schmidt-Mende, Optic Express 20 (2012) A177–A189.
[18] J.J. Hill, N. Banks, K. Haller, M.E. Orazem, K.J. Ziegler, J. Am. Chem. Soc. 133 (2011) 18663–18672.
[19] H.A. Atwater, A. Polman, Nat. Mater. 9 (2010) 205.
[20] A. Polman, H.A. Atwater, Nat. Mater. 11 (2012) 174.
[21] N.M. Ali, N.H. Rafat, Renew. Sustain. Energy Rev. 68 (2017) 212–220.
[22] S.A. Mann, R.R. Grote, R.M. Osgood, A. Alù, E.C. Garnett, ACS Nano 10 (2016) 8620–8631.
[23] J.J. Hill, Photoelectrochemical Energy Conversion in Nanowire-Based Dye-Sensitized Solar Cells: Modeling, Optimization &templated Fabrication, University of Florida, 2010.
[24] E. Stratakis, E. Kymakis, Mater. Today 16 (2013) 133–146.
[25] E. Zimmermann, P. Ehrenreich, T. Pfadler, J.A. Dorman, J. Weickert, L. Schmidt-Mende, Nat. Photon. 8 (2014) 669.
[26] S.R. Cowan, A. Roy, A.J. Heeger, Phys. Rev. B 82 (2010) 245207.
[27] U. Würfel, D. Neher, A. Spies, S. Albrecht, Nat. Commun. 6 (2015) 6951.
[28] L. Schmidt-Mende, J. Weickert, Organic and Hybrid Solar Cells: an Introduction, Walter de Gruyter GmbH & Co KG, 2016.
[29] P. Yu, Y. Yao, J. Wu, X. Niu, A.L. Rogach, Z. Wang, Sci. Rep. 7 (2017) 7696.
[30] A. Giannattasio, I.R. Hooper, W.L. Barnes, 12 (2004) 5881-5886..
[31] H.W. Edwards, R.P. Petersen, Phys. Rev. 50 (1936) 871.
[32] T. Badloe, J. Mun, J. Rho, J. Nanomater. (2017) 18 (2017).
[33] G.F. Burkhard, E.T. Hoke, M.D. McGehee, Adv. Mater. 22 (2010) 3293–3297.
[34] J.L. Hou, A. Fischer, S.C. Yang, J. Benduhn, J. Widmer, D. Kasemann, K. Vandewal, K. Leo, Adv. Funct. Mater. 26 (2016) 5741–5747.
[35] S. Schubert, L. Müller-Meskamp, K. Leo, Adv. Funct. Mater. 24 (2014) 6668–6676.
[36] M. Willenbockel, D. Luftner, B. Stadtmuller, G. Koller, C. Kumpf, S. Soubatch, P. Puschnig, M.G. Ramsey, F.S. Tautz, Phys. Chem. Chem. Phys. 17 (2015) 1530–1548.
[37] G. Zamborlini, D. Lüftner, Z. Feng, B. Kollmann, P. Puschnig, C. Dri, M. Panighel, G. Di Santo, Nat. Commun. 8 (2017) 335.
[38] Q. Tai, F. Yan, Adv. Mater. 29 (2017) 1700192.
[39] S. Schubert, J. Meiss, L. Müller-Meskamp, K. Leo, Adv. Energy Mater. 3 (2013) 438–443.
[40] G.A. dos Reis Benatto, M. Corazza, B. Roth, F. Schütte, M. Rengenstein, S.A. Gevorgyan, F.C. Krebs, Inside or Outside? Linking outdoor and indoor lifetime tests of ITO-free organic photovoltaic devices for greenhouse applications, Energy Technol. 5 (2017) 338–344.